applied optics

Solar eclipse skies and limb reddening

STANLEY DAVID GEDZELMAN

Department of Earth and Atmospheric Sciences and NOAA CREST Center, City College of New York, New York 10031, USA (sdgbrg@gmail.com)

Received 8 May 2020; revised 15 June 2020; accepted 16 June 2020; posted 16 June 2020 (Doc. ID 396964); published 10 July 2020

During solar eclipses the sunlit tops of cloud layers and arctic sea ice near the umbra appear salmon–brown when viewed from airplanes or satellites. Under these conditions, the clouds and atmosphere are illuminated by light restricted to the solar limb, which has effective radiating temperatures as low as 4000 K. The resulting limb reddening largely accounts for the color. A second-order scattering model is used to simulate the color of photographs of cloud tops taken from a flight during the 21 August 2017 eclipse and MODIS Aqua and Terra satellite "true color" images during the 2 July 2019 eclipse. These observed color changes provide data that has potential value in determining the vertical temperature profile of the solar photosphere.

https://doi.org/10.1364/AO.396964

1. INTRODUCTION

One striking atmospheric optical phenomenon seen during total solar eclipses is the reddening of the near-horizon sky, which assumes a color sequence similar to sunrise or sunset even when the eclipsed sun is well above the horizon. The phenomenon is well understood and has been modeled with fidelity to the observations [1–5]. It results in good part because during eclipses light must pass through a greater mean optical thickness of air and aerosol particles to reach an observer in the umbra than to reach an observer in noneclipse conditions, and hence suffers greater than normal loss from Rayleigh and Lorentz–Mie preferential scattering of shorter wavelengths of light.

Many atmospheric optical phenomena are more pronounced and less obscured when viewed from a great height, as from a jet plane, and may also take exaggerated forms [6]. The high vantage point of jets also makes it possible to see the Moon's shadow moving across the earth or clouds below during total solar eclipses. For these reasons, and to ensure a view of the eclipsed sun unobstructed by clouds, Alaska Airlines Great American Eclipse Flight #9671 was dedicated to observing the 21 August 2017 total solar eclipse.

In the minutes before entering the umbra, the top of the cloud layer a few degrees below the horizon assumed a pronounced, lurid orange–brown color, shown in Fig. 1. This observation was first documented by the author [7].

What made the salmon–brown cloud color of Fig. 1 more striking and perplexing was the contrast with sky color. Even within the umbra [Fig. 2] sky color graded from a dark deep blue aloft to a bright off-white with only a faint orange hue just above the horizon. The less pronounced reddening of the near-horizon sky than that seen during numerous other eclipses was due to the relatively 1) narrow umbra (87 km), 2) high cloud top, and 3) high sun, with solar zenith angle, $\boldsymbol{\phi}_{\mathrm{SUN}} = 65.5°$.

Photographs, images, and videos showing similar salmon–brown-colored cloud tops or reddened surface features such as arctic sea ice just outside the umbras of several recent eclipses have been taken from jets near the tropopause [8–11], satellites, and near the surface. The photograph by Eric Adams [12] taken from a drone over Cerro Tololo Inter-American Observatory (lat, lon $= -30.04°$, $-71.30°$) at 2039 UTC with $\boldsymbol{\phi}_{\mathrm{SUN}} = 75.5°$ shows the salmon color of the top of the stratocumulus deck near the horizon at the edge of the umbra of the 2 July 2019 total solar eclipse.

As an anthropological note, we hypothesize that such reddening may have augmented primitive fears regarding total solar eclipses. The apparent "eating" of the sun and darkening was the primary cause of fear, but the attendant reddening adds a haunting, end-of-world quality to it.

The principal cause of the reddening of sunlit cloud tops and surface features just outside the umbras of total solar eclipses is linked to the color of sunlight that reaches Earth at that time, when only a sliver of the Sun's limb is not blocked by the Moon.

Sunlight reaching the Earth from the solar limb is described by the well-known phenomenon of limb darkening [13–15], shown in the photograph of the 05–06 June 2012 Transit of Venus (Fig. 3). To reach Earth, such light must take an oblique path through the solar photosphere and hence originates up to about 300 km higher than light reaching Earth from the solar midpoint. Given the temperature gradient in the photosphere the Sun's effective radiating temperature, $\boldsymbol{T}_{\mathrm{SUN}}$, decreases outward from over 6000 K at the solar midpoint to values in the range of 4000 K to 4500 K at the limb, near the base of the chromosphere.

Models must properly include lower solar radiating temperatures due to limb darkening to correctly simulate solar luminance [16,17] and sky and cloud colors during solar eclipses, and to account for other features of stellar structure.

Fig. 1. Salmon–brown-colored top of cloud deck at the sunward edge of the penumbra at 1700 UTC 21 August 2017 facing east.

Fig. 2. Edge of the umbra of 21 August 2017 eclipse at 1701 UTC. The umbra was too narrow and the Sun too high to produce significant reddening of the near horizon sky.

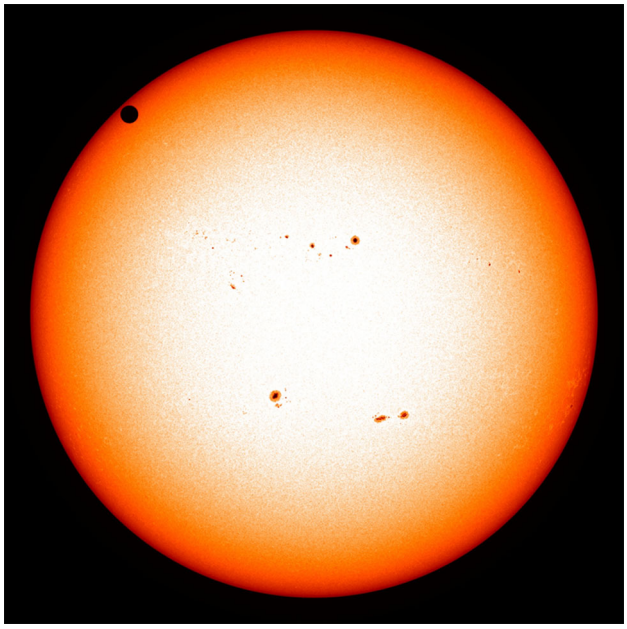

Fig. 3. Limb darkening and reddening during the 2012 transit of Venus with sunspots and granulation visible. NASA Image HMIintensity_WholeSun_2k_20120605T222847.

For example, limb darkening is used to determine stellar diameters by combining center to limb darkening profiles with interferometer measurements of the light from stars [18].

The degree of limb darkening, which was first measured in the late 1800s [19], is wavelength dependent, with peaks around various absorption and emission lines in the ultraviolet and infrared. However, in the visible light range, the gradient of limb darkening decreases monotonically with wavelength in such a way that closely matches changes of Planck radiation resulting from lower limb temperatures [19,20]. In turn, this implies that limb darkening may also be called "limb reddening," a term coined by Lites [21], and therefore that the sunlight just outside the umbra of solar eclipses is not only dimmer but redder than normal. Limb reddening is clearly seen in Fig. 3.

The purpose of this paper is to document, explain, and simulate the salmon–brown color of the cloud tops and reddening of surface features observed near the umbras of solar eclipses. We first present and discuss the data from sources consisting of images and meteorological parameters obtained from satellites, soundings, and models. The second-order scattering model that includes solar limb reddening is described, and the simulated color and light features are then presented and discussed.

2. SATELLITE IMAGERY AND METEOROLOGICAL OBSERVATIONS

Photographs and videos provide dramatic documentation of the reddening of the near horizon sky, clouds, and surface features in and near the umbra of solar eclipses, while satellite images provide quantitative data and cover much greater areas. For example, the NOAA GOES West infrared satellite image at 1700 UTC 21 August 2017 (Fig. 4) shows a band of midlevel clouds with cloud top temperature $\approx -3°C$ at the time and place Flight #9671 entered the umbra (44°N, 141°W). NOAA Atmospheric Research Labs (ARL) GDAS1 soundings for 1800 UTC were consistent with a cloud top pressure, $p_{CLD} \approx 600$ hPa.

MODIS Terra and Aqua polar orbiting satellites, which scan with small angles around the nadir, provide not only "true color" visible images but more detailed and higher-resolution quantitative data of many parameters, albeit with incomplete

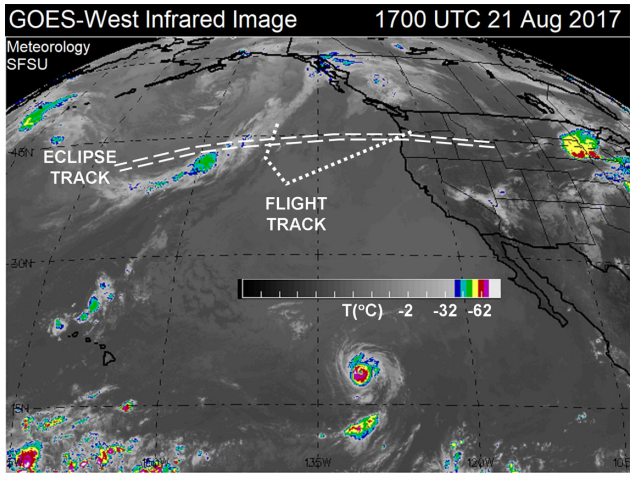

Fig. 4. GOES-West Infrared Image at 1700 UTC 21 August 2017 with the eclipse track (dashed double line) and its intersection with the outbound flight track (dotted line).

coverage. Images and data are available at https://worldview.earthdata.nasa.gov/. The Terra and Aqua satellites make diurnal overpasses around 1000 and 1400 local time, respectively. Each of these satellites has a different orbit, which increases total coverage but makes it unlikely for both satellites to see the same small-scale and transient phenomena.

The MODIS Terra Image at 2105 UTC 21 August 2017 shows the cloud band 4 h after Fig. 1. Cloud top temperature ranged from ≈5°C at the cloud band's eastern edge to ≈−18°C 100 km further west, bracketing the cloud top temperature of Fig. 4 when the flight entered the umbra.

MODIS satellites measure the vertically integrated aerosol optical thickness, τ_{AER}, and the aerosol index. τ_{AER} is measured only where there are no clouds. Coverage is spotty, and the vertical structure of aerosol concentration can be determined only if an elevated plume casts a shadow. The aerosol indices over larger regions of the Pacific Ocean near the umbras of the eclipses of 21 August 2017 and 2 July 2019 had values near 0 that are typical of marine aerosols.

In clean air ($\tau_{AER} \ll 1$) MODIS "true color" images are designed to show how the surface and cloud tops would appear to observers standing or flying immediately overhead. The images are processed with an algorithm that removes the effects of Rayleigh scattering between the surface or cloud top and the satellite [22]. Scattering and absorption due to aerosol particles are retained so that smoke plumes and haze stand out by coloring or obscuring surface features in MODIS images.

When there are no elevated haze layers or smoke plumes, cloud tops, sun glint, snow, and ice appear white in almost all MODIS images. In clean air it is only near the umbras of solar eclipses that MODIS images show tan sun glint and tan or brown cloud tops (Fig. 5), and reddened surface features such as sea ice (Fig. 6). In general, the closer to the umbra and the lower the surface, the deeper the red or brown tint.

The height dependence of cloud-top color is illustrated by the 26 December 2019 Aqua image of Typhoon Phanfone in the penumbra of the annular eclipse at 0600 UTC in Fig. 5(b). The low-level clouds on the periphery of the typhoon are deeper brown than the higher central dense overcast and spiral bands. Given that the cloud tops of the central dense overcast extended above the top of the sounding at 100 hPa (≈17000 m) with the sun high in the sky ($34° \le \phi_{SUN} \le 50°$), scattering losses in the atmosphere were so small that the tan color could be caused only by limb reddening. In Fig. 5(c) the Terra image of Typhoon Phanfone 3 h before the eclipse at 0255 UTC shows that all cloud tops were white.

The impact of the proximity to the umbra on the color and brightness of sea ice for the 20 March 2015 eclipse is shown in Fig. 6. This image was taken roughly 13 min after the end of totality, and the umbra had moved off to the upper right of the image, where the sea ice and clouds appeared both reddest and darkest.

The proximity to the umbra also leads to deeper salmon–brown cloud tops, as indicated by images of both high clouds for the 21 August 2017 eclipse and low clouds for the 2 July 2019 eclipse. The color of the cirrostratus cloud tops in the Terra image of 1745 UTC 21 August 2017 (Fig. 7) graded from near white over Lake Superior to tan farther west over Nebraska and closer to the umbra. The cloud top pressure of 200 hPa, as indicated by the NOAA ARL GDAS1 soundings, was almost constant, and the MODIS derived cloud optical thickness was also constant. At the same time, the surface features over SE Utah and NE Arizona at the bottom left of the image were much deeper red than for noneclipse times.

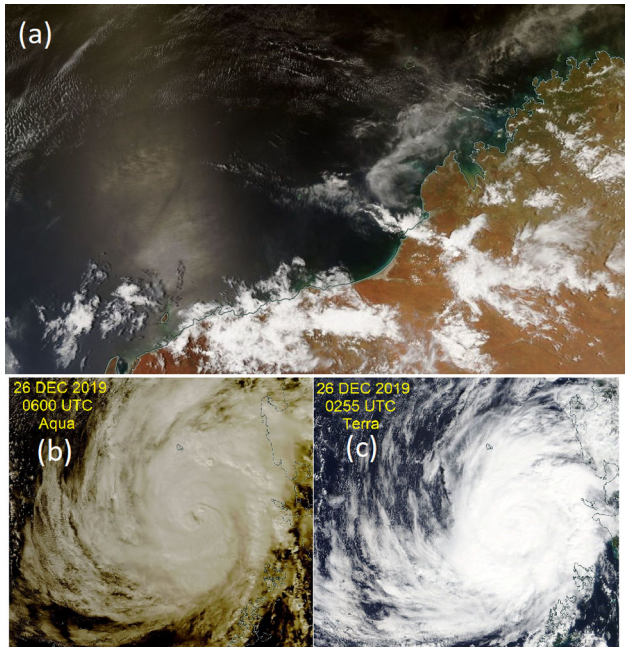

Fig. 5. (a) Tan-colored sun glint north of W. Australia in the MODIS Aqua "true color" image at 0600 UTC during the eclipse of 26 December 2019. (b) MODIS Aqua image of Typhoon Phanfone during, and (c) MODIS Terra image 3 h before, the eclipse.

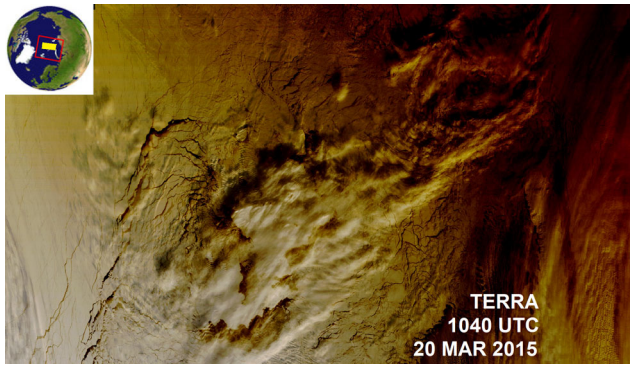

Fig. 6. MODIS Terra Image, 1040 UTC 20 March 2015 of reddened Arctic Ocean sea ice and clouds 13 min after totality. The yellow rectangle in the inset map shows the area of the image.

In the MODIS Aqua image of 2 July 2019 (Fig. 8), the stratocumulus cloud tops over the subtropical Pacific Ocean west of South America appeared normally white in the overpass at 1820 UTC prior to the eclipse on the eastern side of Fig. 8, but had a brown hue that deepened toward the umbra where sunlight was confined to the narrowing sliver of the solar limb during the eclipse at 1955 UTC when $\phi_{SUN} \approx 45°$. Cloud top pressure was an almost constant 900 hPa throughout the entire region east and south of the umbra as indicated by NOAA ARL GDAS1 soundings.

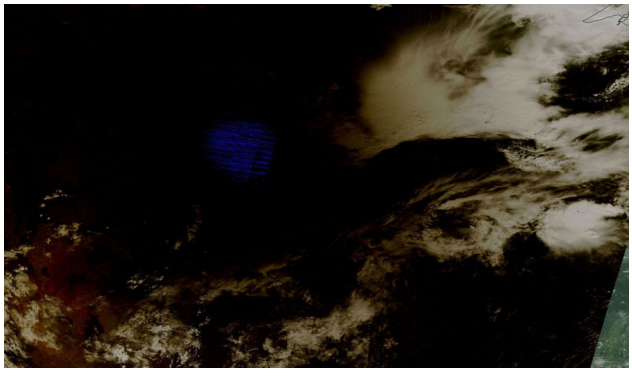

Fig. 7. Terra Image of 1745 UTC 21 August 2017 of cirrostratus cloud top grading from near white over Lake Superior at upper right to deep tan over Nebraska closer to the umbra (blue region). The land surface over SE Utah and NE Arizona at lower left is much deeper red than normal.

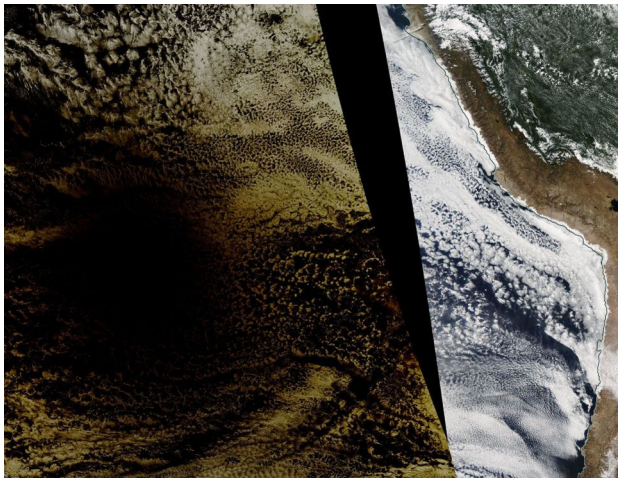

Fig. 8. MODIS Aqua composite image showing stratocumulus cloud tops brown in the penumbra at 1955 UTC 2 July 2019 over the subtropical Pacific Ocean west of South America that contrast with the normally white tops shown in the 1820 UTC satellite pass (at right) over South America before totality.

Measuring the color gradient of the cloud tops with distance from the umbra holds potential value for solving an inverse problem, the vertical temperature gradient in the solar photosphere. Quantitative data from the visible light and short infrared channels of the MODIS satellites are amenable to such analyses.

3. MODEL

The model used here represents an extension of a model used to simulate sky colors during normal and eclipse conditions [4]. Sunlight at 61 uniformly spaced visible wavelengths from $0.4\ \mu\text{m} \leq \lambda \leq 0.7\ \mu\text{m}$ is depleted by absorption in the stratosphere in the Chappuis Bands of ozone and attenuated by scattering in its passage through the atmosphere. Model skylight consists of single scattered sunlight that suffers loss from a second scattering on its path through the atmosphere. Neglect

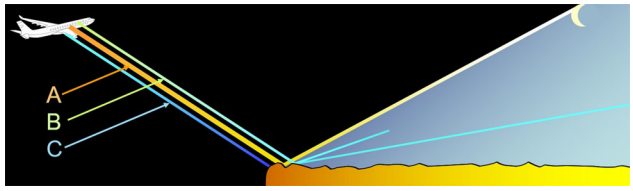

Fig. 9. Three simulated components of light reaching an elevated observer: A) sunlight reflected from the cloud, B) skylight reflected from the cloud, and C) skylight between cloud and observer. The black region represents the umbra.

of the typically small contributions of higher-order scattering to skylight causes a blue bias that is small in most cases but produces enormous time savings for model runs, which take only seconds. The model includes Earth's curvature, but since it is only two-dimensional, results are confined to the vertical plane that includes the Sun and the observer.

The simulated illumination and color of a cloud top or surface feature seen by an observer includes three components, illustrated in Fig. 9. Component A, direct sunlight reflected from the cloud top, has a red tint as a result of the long passage of sunlight through the atmosphere to cloud top and then continues as reflected light to the observer. Component B, skylight reflected from the cloud top, grades from pale blue directly below the observer to pink near the horizon. Component C, skylight between the cloud and the observer, is bluest because it consists of scattered sunlight and suffers the least depletion by a second scattering.

The relative magnitudes of the components depend on the proximity to the umbra. Reflected sunlight (component A) dominates, except in or at the edge of the umbra, where distant skylight (component B) dominates because there is little or no sunlight and no scattered light in the umbra between the cloud and the observer. As a result, the cloud within the umbra tends to appear dark gray and not salmon–brown, as is seen in Fig. 2.

The model's free parameters include black body temperature of the Sun's limb, $\boldsymbol{T}_{\text{SUN}}$, solar zenith angle, $\boldsymbol{\phi}_{\text{SUN}}$, observing zenith angle, $\boldsymbol{\phi}_{\text{OBS}}$, pressure of the cloud top, $\boldsymbol{p}_{\text{CLD}}$, and observer, $\boldsymbol{p}_{\text{JET}}$, height of the edge of the umbra above the observer, $\boldsymbol{h}_{\text{UMB}}$, cloud albedo, $\mathbf{Alb}_{\text{CLD}}$, ozone content, and atmospheric turbidity, $\boldsymbol{\beta}$, defined as the ratio of the optical thicknesses of the turbid to the molecular atmosphere. All simulations presented in the next section used 300 Dobson units of ozone. Rayleigh scattering by air molecules is assumed proportional to $\boldsymbol{\lambda}^{-4}$. Lorentz–Mie scattering by aerosols is assumed proportional to $\boldsymbol{\lambda}^{\alpha}$, where we used the mean observed value of the Ångström exponent, $\alpha = -1$ [4,23]. Scattering by such aerosols deepens reddening of cloud tops and surface features because it varies inversely with wavelength.

4. SIMULATIONS

We now simulate the apparent color of sunlit cloud tops for the eclipses of 21 August 2017 and 2 July 2019. The salmon–brown color of cloud tops and reddening of surface features in the "true color" satellite images and photographs that deepen near the

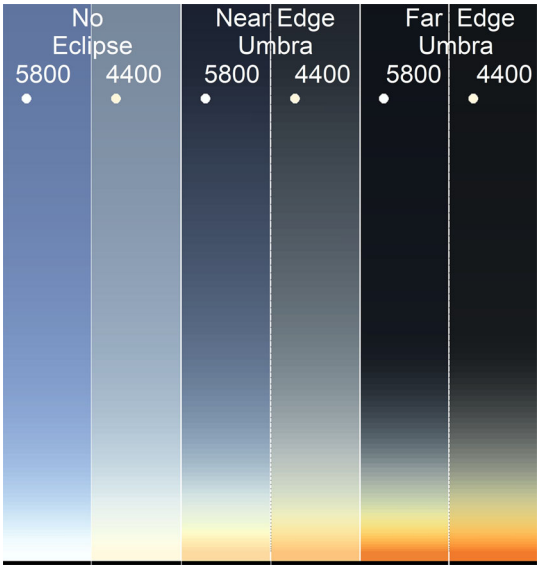

Fig. 10. Panels of simulated sky color and brightness profiles for $54^\circ < \phi_{OBS} < 92.1^\circ$ for three pairs of situations matching flight conditions for the 21 August 2017 eclipse. The left member of each pair shows the sky for $T_{SUN} = 5800$ K, the right member, for $T_{SUN} = 4400$ K. The left pair is for noneclipse conditions, the central and right pairs are for the near and far edges of the umbra. Brightness of each panel is independent.

umbras in eclipses suggest that the effective radiating temperature of the solar limb, T_{SUN}, is the critical parameter, and the simulations confirm this.

In general, the lower the Sun's effective radiating temperature and the longer the optical path light must take through the atmosphere to reach the observer the redder the sky, cloud top, and surface will appear. The reddest cloud tops and surface features therefore occur 1) nearest the horizon, 2) nearest the umbra, 3) when the sun is lowest in the sky, 4) when the cloud top is lowest in the troposphere, and 5) when viewed from a great height above cloud top or surface.

The model is first used to simulate sky color from the horizon to the zenith. Figure 10 displays the results of six simulations of sky color and relative brightness for the conditions of Flight #9671 into the 21 August 2017 eclipse, namely, from the visible horizon at $\phi_{OBS} = 92.1^\circ$ up to $\phi_{OBS} = 54^\circ$, for $\phi_{SUN} = 65.5^\circ$, $p_{CLD} = 600$ hPa, $p_{JET} = 250$ hPa (respectively, about 4000 m and 11,000 m above mean sea level), and $\beta = 1.0$. At that time, umbral width was 87 km.

Figure 10 contains three pairs of panels of simulated sky brightness. Each pair compares the sky with $T_{SUN} = 5800$ K to that with $T_{SUN} = 4400$ K. The left pair represents noneclipse conditions. The center and right pairs show the sky at sunward and opposite edges of the umbra, respectively. Sky brightness is relative within each panel. If an absolute brightness scale were used, panels with $T_{SUN} = 4400$ K would be much darker than panels with $T_{SUN} = 5800$ K, and panels for the normal conditions would be much brighter than those for eclipse conditions.

For noneclipse conditions with $T_{SUN} = 5800$ K color grades from near white at the horizon to a blue that deepens toward the zenith. But when $T_{SUN} = 4400$ K, the sky under noneclipse

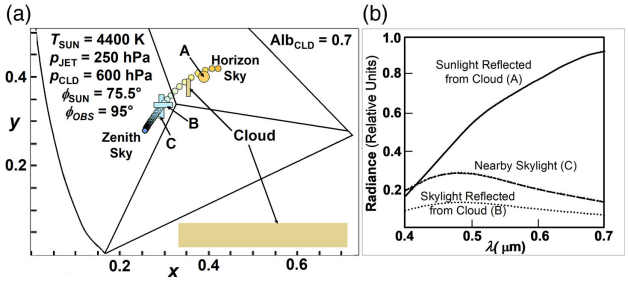

Fig. 11. (a) Chromaticity diagram showing simulated sky color from horizon to zenith (string of circles) and contributions A, B, and C (described in the text) for apparent cloud top color (labeled Cloud) for conditions of Fig. 1, assuming $\beta = 1.0$, $\mathbf{Alb}_{CLD} = 0.7$, and $h_{UMB} = -10$ km. (b) Spectra of relative radiance of contributions, A, B, and C.

conditions would appear pale orange at the horizon and grade to pale blue above. For eclipse conditions, the sky just above the horizon is redder and deepest red when viewed from the far side of the umbra, as is observed, because much light originates further from the sunward umbra edge. However, comparing the central panels of Fig. 10 to Fig. 1 shows that the simulated skies are somewhat too red just above the horizon, because the model extinguishes skylight that is scattered more than once.

The model is next used to simulate cloud-top color during eclipse conditions. Even under noneclipse conditions distant sunlit clouds appear pink because reflected sunlight (component A) dominates at all times. During eclipses distant sunlit clouds appear redder largely because of limb reddening. The relative magnitude of distant skylight (component B) is larger but remains small during eclipses because solar illumination and sky brightness increase with distance from the umbra. For the same reason, interposing skylight between cloud and observer (component C) is less than normal because it is closer to the umbra.

Figure 11(a) shows the simulated chromaticity of sky color from horizon to zenith (small circles) and cloud top color for conditions near the sunward edge of the umbra ($h_{UMB} = -10000$ m) during Flight #9671 into the 21 August 2017 eclipse for an observer facing 5° below horizontal ($\phi_{OBS} = 95^\circ$) for $\beta = 1.0$, cloud albedo, $\mathbf{Alb}_{CLD} = 0.7$, and $T_{SUN} = 4400$ K. Components B and C both contribute blue light but the orange sunlight reflected from the cloud (component A) dominates and causes the salmon–brown color. For optically thin clouds ($\mathbf{Alb}_{CLD} \leq 0.25$) much less sunlight is reflected, so component C dominates and cloud color is not salmon.

Figure 11(b) shows spectra of the relative magnitudes of the three components for $\mathbf{Alb}_{CLD} = 0.7$. Sunlight reflected from the cloud (A) is the major component of light reaching the observer at all values of T_{SUN}. The model overestimates the contribution of skylight reflected from the cloud (B) because it is two-dimensional and skylight directly facing the Sun originates on average further from the umbra than skylight originating at other azimuth angles. This gives the simulated cloud colors for the sunward side of the penumbra a small blue bias.

Most of the simulations presented in this section were run for a molecular atmosphere ($\tau_{AER} = 0$, $\beta = 1.0$), because

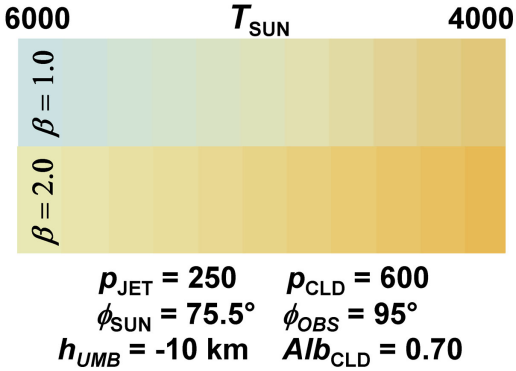

Fig. 12. Simulated cloud-top color as a function of T_{SUN} at the sunward edge of the umbra for conditions of Fig. 1 with $\phi_{OBS} = 95°$, for atmospheric turbidity, $\beta = 1.0$, and $\beta = 2.0$ ($\tau_{AER} \approx 0.06$).

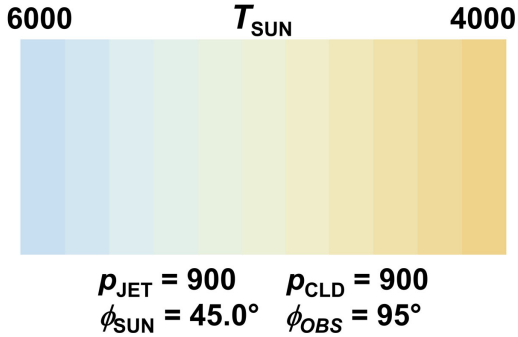

Fig. 13. Simulated Aqua image of cloud-top color as a function of T_{SUN} in the penumbra for conditions at 1955 UTC 2 July 2019.

effective values of τ_{AER} for the two eclipses above cloud tops were quite small. MODIS measured values ranged from $0.040 < \tau_{AER} < 0.045$ near the umbra edge of Flight #9671 on 21 August 2017 and $0.001 < \tau_{AER} < 0.060$ near the umbra of the 2 July 2019 eclipse. Although elevated aerosol layers do occur, the typical vertical aerosol profile has a maximum at the surface and a scale height of 2.5 km. Therefore, most of the aerosols were likely confined below the cloud top so that for these eclipses $\tau_{AER} < 0.01$ or, $\beta < 1.1$ above the cloud top. Furthermore, the small measured aerosol indices indicated typical marine aerosols (Ångström exponent, $\alpha \approx -1.1$ [23]), which would add only minor additional reddening. However, to show the potential reddening that aerosols can produce when atmospheric turbidity is significant, simulated cloud colors were calculated for $\beta = 2.0$ and compared to colors for $\beta = 1.0$ in Fig. 12.

Figure 12 shows the dependence of cloud-top color just inside the umbra of Flight #9671 on the temperature of the solar limb for $\beta = 1.0$ and $\beta = 2.0$. In a molecular atmosphere ($\beta = 1.0$) the color grades from pale blue for $T_{SUN} = 6000$ K to salmon–orange when $T_{SUN} = 4000$ K and cloud tops are orange for solar limb temperatures, $T_{SUN} \leq 5000$ K. In the turbid atmosphere ($\beta = 2.0$) the cloud top appears deeper orange at all values of T_{SUN} and is yellow for $T_{SUN} = 6000$ K.

Cloud-top color was also simulated as a function of T_{SUN} for $\beta = 1$ and conditions shown by the Aqua satellite at 1955 UTC of the eclipse of 2 July 2019 (Fig. 13). At the time of the image, $\phi_{SUN} = 45°$ and stratocumulus clouds with $p_{CLD} \approx 900$ hPa covered a wide area of the subtropical eastern South Pacific. This simulation places the observer at the cloud top, $p_{OBS} = 900$ hPA, making results independent of ϕ_{OBS}, because the MODIS "true color" images filter out Rayleigh scattering between the surface or cloud top and the satellite.

The simulated cloud-top colors range from turquoise at $T_{SUN} = 6000$ K to orange at $T_{SUN} \leq 4800$ K. Given that $p_{CLD} = 900$ hPA was constant and aerosol content was low over the entire region, as is typical in the descending air of the South Hemisphere Subtropical Pacific High, the color gradient in the Aqua image must be attributed almost entirely to the lower effective values of T_{SUN} in the outer fringes of the exposed solar limb approaching the umbra.

5. SUMMARY AND DISCUSSION

This paper was inspired by the observation of a striking, dull salmon–orange color of the top of a sunlit cloud layer near the umbra of the eclipse of 21 August 2017 seen from Alaska Airlines Great American Eclipse Flight #9671.

Similar reddening of cloud tops and surface features is documented by photographs and satellite images, in particular of the MODIS Terra and Aqua satellites, which have three channels in the visible. Cloud tops appear as a salmon–orange color in photographs and as a brown color that darkens and deepens in tone toward the umbra in the MODIS images, where light comes from a thinner outer sliver of the solar limb.

During solar eclipses the light reaching the edge of the umbra derives entirely from a sliver of the solar limb. The oblique path that sunlight must take through the limb to reach Earth means that light arrives from near the top of the photosphere, where temperatures are as low as 4000 K. This leads to the well-known phenomenon of limb darkening, which can also be called limb reddening. The cooler, redder sunlight from the limb reddens the sky and any illuminated object such as cloud tops and surface features.

The reddening was simulated using a double scattering model. Model runs showed that the primary factor is the lower effective radiating temperature of the solar limb, which becomes marked in a molecular atmosphere for effective solar radiating temperatures below about 5000 K and for higher temperatures when aerosols are included. A secondary but still important factor is that skylight during the eclipse increases outward from the umbra so that any light reaching an observer in or near the umbra must pass through a greater optical thickness of air than normal, so that it is reddened by scattering losses that are largest at small wavelengths.

The model has several limitations. All light reaching the observer is single scattered or reflected light that is depleted by scattering on its path to the observer. This produces a small red bias. The calculated radiance of skylight reflected from the cloud is based on a cylindrical model of the earth that in eclipse conditions represents an overestimate. This produces a small blue bias. Including aerosols reddened the apparent cloud-top color.

In ancient times eclipses inspired awe and fear. This was certainly due to the apparent "eating" of the Sun and the turning of day into night. But the reddening or browning adds a weird

tone to the sky and landscape that may have increased any sense of discomfort. Even today, eclipses continue to inspire and provide information not otherwise easily available. For example, the progressive reddening of cloud tops toward the umbra has potential value in determining the vertical temperature profile of the photosphere.

Acknowledgment. I particularly thank Joseph Rao for wrangling seats for my wife and me aboard Alaska Airlines Flight #9671 that led to the observation that inspired this paper. I am grateful to and praise the staff and executives at Alaska Airlines for creating and funding the dedicated eclipse flight. As always, I thank my colleagues for their insights that have added so much to my knowledge of atmospheric optics over the years. Drs. Michael Vollmer and Joseph Shaw in particular made several important points that improved the paper. Finally, I thank the anonymous reviewers for the necessary troubles they give me to eliminate errors, improve clarity, and turn fiction into science.

Disclosures. The author declares no conflicts of interest.

REFERENCES

1. J. Q. Stewart and C. D. MacCracken, "The general illumination during a total solar eclipse," Astrophys. J. **91**, 51–71 (1940).
2. G. Shaw, "Sky brightness and polarization during the 1973 African eclipse," Appl. Opt. **14**, 388–394 (1975).
3. S. D. Gedzelman, "Sky color near the horizon during a total solar eclipse," Appl. Opt. **14**, 2831–2837 (1975).
4. S. D. Gedzelman, "Simulating colors of clear and partly cloudy skies," Appl. Opt. **44**, 5723–5736 (2005).
5. C. Emde and B. Mayer, "Solar radiation during a total eclipse," Atmos. Chem. Phys. **7**, 2259–2270 (2007).
6. J. Shaw, *Optics in the Air: Observing Optical Phenomena through Airplane Windows* (SPIE, 2017).
7. S. D. Gedzelman, "View from the top: studying the 2017 total solar eclipse on the flight to nowhere," Weatherwise **71**, 26–32 (2018).
8. S. Chapeland, "What March's total solar eclipse looked like from an airplane window," 2015, https://twistedsifter.com/videos/march-total-solar-eclipse-from-an-airplane-window/.
9. Aerotime Extra Staff, "Video shows solar eclipse from Alaska Airlines flight," 2017, https://www.aerotime.aero/aerotime.extra/23114-video-shows-solar-eclipse-from-alaska-airlines-flight.
10. W. Curtiss, and Alaska Airlines Blog, "Threading the celestial needle: catching the great American eclipse at 35,000 feet," 2017, https://blog.alaskaair.com/alaska-airlines/solar-eclipse/.
11. Egypt Independent, "South Americans marvel at total solar eclipse," 2019, https://egyptindependent.com/south-americans-marvel-at-total-solar-eclipse/.
12. E. Adams, "A drone, a $12,000 lens, and the magic of a total solar eclipse," Wired Magazine, 2019, https://www.wired.com/story/south-america-total-solar-eclipse-2019/.
13. E. A. Milne, "Radiative equilibrium in the outer layers of a star: the temperature distribution and the law of darkening," Mon. Not. R. Astron. Soc. **81**, 361–375 (1921).
14. H. Neckel and D. Labs, "Solar limb darkening 1986-1990," Solar Phys. **153**, 91–114 (1994).
15. J. Aufdenberg, "Stellar atmospheres and surfaces," 2006, https://nexsci.caltech.edu/workshop/2006/talks/Aufdenberg.pdf.
16. K.-P. Möllmann and M. Vollmer, "Measurements and predictions of the illuminance during a solar eclipse," Eur. J. Phys. **27**, 1299–1314 (2006).
17. M. Vollmer, "Solar and lunar eclipses: observations, measurements, and quantitative models," Praxis d. Naturwiss. Physik **58**, 38–44 (2009).
18. I. Howarth, "On stellar limb darkening and exoplanetary transits," Mon. Not. R. Astron. Soc. **418**, 1165–1175 (2011).
19. G. Muller, *Die Photometrie der Gestirne* (W. Engelmann, 1897).
20. D. Hestroffer and C. Magnan, "Wavelength dependency of solar limb darkening," Astron. Astrophys. **333**, 338–342 (1998).
21. B. Lites, "An estimation of the fluctuations in the extreme limb of the Sun," Solar Phys. **85**, 193–214 (1983).
22. "SSEC Polar2Grid reader: corrected reflectance reader," https://www.ssec.wisc.edu/software/polar2grid/readers/crefl.html.
23. C. Toledano, V. Cachorro, A. Berjon, A. de Frutos, M. Sorribas, B. de la Morenab, and P. Goloub, "Aerosol optical depth and Ångström exponent climatology at El Arenosillo AERONET site (Huelva, Spain)," Q. J. R. Meteorol. Soc. **133**, 795–807 (2007).